Chinese Chemical Letters 36 (2025) 109911

Contents lists available at ScienceDirect

Chinese Chemical Letters

journal homepage: www.elsevier.com/locate/cclet

A wearable sensor device based on screen-printed chip with biofuel cell-driven electrochromic display for noninvasive monitoring of glucose concentration

Kezuo Di[a], Jie Wei[a], Lijun Ding[b], Zhiying Shao[b], Junling Sha[a], Xilong Zhou[a], Huadong Heng[a], Xujing Feng[a], Kun Wang[a,*]

[a] School of Chemistry and Chemical Engineering, Jiangsu University, Zhenjiang 212013, China
[b] Key Laboratory for Theory and Technology of Intelligent Agricultural Machinery and Equipment, Jiangsu University, Zhenjiang 212013, China

ARTICLE INFO

Article history:
Received 12 March 2024
Revised 17 April 2024
Accepted 19 April 2024
Available online 20 April 2024

Keywords:
Wearable flexible sensor device
Electrochromic display
Visualization
Biofuel cell
Screen-printed chip

ABSTRACT

Wearable flexible sensor devices have the characteristics of lightweight and miniaturization. Currently, power supply and detection components limit the portability of wearable flexible sensor devices. Meanwhile, conventional liquid electrolytes are unsuitable for the integration of sensing devices. To address these constraints, wearable biofuel cells and flexible electrochromic displays have been introduced, which can improve integration with other devices, safety, and color-coded display data. Meanwhile, electrode chips prepared through screen printing technology can further improve portability. In this work, a wearable sensor device with screen-printed chips was constructed and used for non-invasive detection of glucose. Agarose gel electrolytes doped with PDA-CNTs were prepared, and the mechanical strength and moisture retention were significantly improved compared with traditional gel electrolytes. Glucose in interstitial fluid was non-invasive extracted to the skin surface using reverse iontophoresis. As a biofuel for wearable biofuel cells, glucose drives self-powered sensor and electrochromic display to produce color change, allowing for visually measurement of glucose levels in body fluids. Accurate detection results can be visualized by reading the RGB value with a cell phone.

Wearable flexible sensor devices (WFSDs) are designed to monitor health indicators in real-time [1] and offer the convenience of being lightweight, compact, and flexible, enhancing user comfort and ease of use [2]. They operate using chemical sensors [3] that non-invasively analyze body fluids such as sweat, interstitial fluid (ISF), and saliva [4], thereby reducing the risk of discomfort and infection associated with traditional sampling methods [5]. However, current wearable technologies face challenges related to their size and rigidity, particularly in power supply and detection components [6]. Moreover, the use of batteries containing harmful chemicals may present health risks [7]. To address these issues, wearable devices are being developed with sustainable, biocompatible, and self-powered features, along with user-friendly displays for immediate monitoring feedback, aiming for a balance of reliability, portability, and simplicity.

Among the various self-powered wearable devices such as piezoelectric generators, supercapacitors, and friction nanogenerators [8], wearable biofuel cells (w-BFCs) are uniquely functional and biocompatible [9]. Since w-BFCs are based on the reaction of biological components in natural fuels to generate green energy, they are virtually harmless even when they come into close contact with the user [10]. Physiological fluids such as sweat, tears, and interstitial fluid (ISF) [11] are easily obtainable under wearable conditions. These physiological fluids can be used to collect physiological markers like glucose, lactate, and ethanol [12]. The concentration of physiological markers can be analyzed based on the output signal of wearable biofuel cells (w-BFCs). Therefore, the w-BFCs are considered the best candidates to power WFSDs [13]. The combination of a power supply unit and a detection unit using w-BFCs [14] enables the production of green bioenergy from detected substances. To sum up, the w-BFCs have good wearable performance and meet the requirements of environmental friendliness and biocompatibility.

On the other hand, the introduction of visualization aligns better with human common sense. The currents generated by w-BFCs can be used to communicate sensor data more intuitively through visualization techniques without the need for large external instruments to display them. The data can be analyzed by simply reading

* Corresponding author.
E-mail address: wangkun@ujs.edu.cn (K. Wang).

https://doi.org/10.1016/j.cclet.2024.109911
1001-8417/

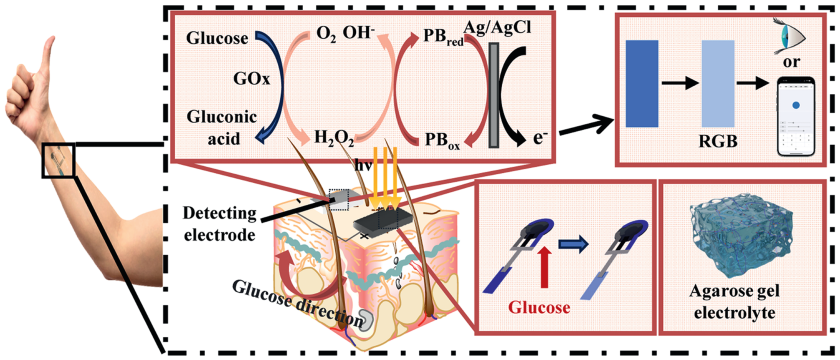

Scheme 1. Schematic diagram of the device principle and the way to visualize and read the test results of the WFSD designed in this design for testing human glucose concentration.

the colors with the naked eye. Visualization employs color or light emission to convert electrical signals or mechanical forces into optical signals [15]. Therefore, by plugging visualization displays into w-BFCs and using them in combination with WFSDs, the size of the initial device can be reduced. This allows for data to be collected anytime and anywhere for real-time monitoring without the need for bulky external detection equipment and power supplies. Visualization is typically achieved through techniques such as electrochromic (EC), photochromic, and stress detection [16], among others. Among them, the wearable electrochromic device technology [17] has been widely studied due to its unique wearability, where actions such as bending and stretching during daily wear do not degrade its performance [18] and has been widely used for visualization purposes in WFSDs.

The output current of w-BFCs is sufficient to drive EC displays. While the role of w-BFCs and the color change of EC displays require electrolytes to transmit electrons [19]. Agarose, a natural extract from seaweed, is non-toxic and ideal for electrolytes in WFSDs devices [20]. Unfortunately, the lack of moisturizing properties of agarose gel electrolyte limits their long-term use. To address this issue, water-retaining materials should be added to the gel to enable reuse of WFSD.

Diabetes is one of the most serious diseases and has a great impact on the health of the patient [21]. Currently, the most common way of self-testing is blood glucose testing. During the blood collection process, patients need to endure pain and the wound is not easy to heal, leading to secondary infection. ISF is an extracellular fluid that fills the outside of the cells [22] and contains nutrients that come from the capillaries [23] and is therefore related to the bloodstream [24]. More importantly, the concentration of glucose in ISF is almost the same as that at blood glucose equilibrium and changes rapidly. It provides a better alternative for non-invasive testing. Utilizes reverse iontophoresis (RI) [25] to non-invasively extract glucose from ISF, avoiding the drawbacks of traditional blood glucose meter testing. Glucose serves as both fuel and detector for the device, allowing for wearable, noninvasive glucose monitoring.

Herein, A schematic diagram of the detection mechanism and experimental setup was shown in Scheme 1. The device was affixed to the upper arm of the human body. All these electrodes were fabricated on PET film using the simplest and easiest screen-printing process to produce screen-printed chips (SPCs) for WFSDs. The photoelectric material at the positive electrode of the WFSDs generated photocurrent upon illumination, which makes the skin surface somewhat negatively charged, and the resulting potential induces the anions to move toward the anode, and the cations and the central molecule to move toward the cathode; this is electromigration and electro-osmosis. Since glucose molecules are not electrically charged, glucose is transported through RI. Subsequently, the glucose transported to the negative electrode (detection electrode) reacts with the enzyme electrode through the delivery of the gel electrolyte. Under the catalysis of glucose oxidase (GOx) and oxygen, glucose was converted into hydrogen peroxide and gluconic acid, with the generated hydrogen peroxide effectuating the transformation of PB_{red} to its PB_{ox} form, which released electrons in the presence of Ag/AgCl to produce an electric current [26]. The biofuel glucose-based battery reacts to varying degrees depending on the concentration of glucose, which resulted in differences in the magnitude of the discharge, and consequently, the magnitude of the current entering the electrochromic display. Finally, the color of the electrochromic display will change depending on the concentration of glucose. If a specific value was needed, the RGB can be obtained by taking a picture with a cell phone and calculating the glucose.

To prepare the WFSD, agarose gel electrolyte doped with PDA-CNTs and SPCs were prepared and assembled respectively. The specific apparatus and equipment materials were mentioned in Supporting information.

As shown in Fig. S1 (Supporting information), 15.2 mg of dopamine hydrochloride was mixed with 20 mg of CNTs, and 40 mL of Tris–HCl was added, and then stirred for 12 h. The mixture was centrifuged at 15,000 rpm for 5 min and washed three times with deionized water. The PDA-CNTs was obtained after drying at 60 °C and added to the agarose solution dissolved at 150 °C to prepare the agarose gel electrolyte doped with PDA-CNTs. Then, the agarose gel electrolyte doped with PDA-CNTs was applied to the two electrodes of the reverse iontophoresis electroosmosis, ensuring that the gel electrolyte was first in contact with the skin.

To obtain wearable flexible electrodes, the screen-printing technology was prepared to the electrodes. As shown in Fig. S2 (Supporting information), PET film with a thickness of 0.05 mm was selected as the base of the SPCs, and conductive carbon paste, Prussian blue and Ag/AgCl electrodes were printed respectively. After completed, the PET films were dried at 120 °C for 6 h. The three electrodes used for detection were obtained by cutting the electrodes with a cutting machine. SPCs were obtained by assembling these electrodes.

Fig. S3 (Supporting information) is a schematic diagram of the assembly of the experimental setup. First, a Prussian blue flexible electrochromic display was connected outside the SPCs for color development, and nail polish was applied to the three electrodes as an insulating material. Subsequently, the RI electrode was assembled into the working electrode, where the hollow was designed to allow the agarose gel electrolyte to cover the RI electrode to avoid direct contact with the skin. Finally, the agarose gel electrolyte was covered on the two RI electrodes and the Prussian blue electrochromic display, respectively. At this point, the WFSD was successfully assembled.

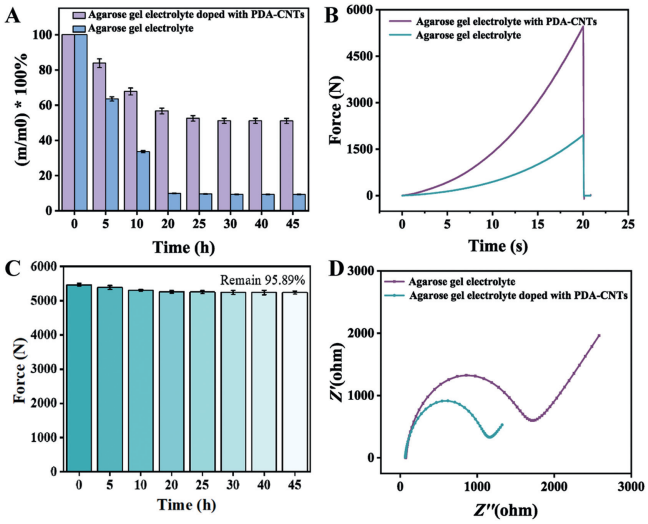

Fig. 1. (A) Water retention and (B) compression resistance curves of agarose gel electrolyte doped with PDA-CNTs and agarose gel electrolyte. (C) Plots of compression resistance of agarose gels with PDA-CNTs after different time periods. (D) EIS Nyquist plots of agarose gel electrolyte doped with PDA-CNTs and gel electrolytes.

After assembled, the equipment for this work was tested in detail. Initially, the morphologies of the CNTs and PDA-CNTs were investigated by SEM and TEM in Fig. S4 (Supporting information). As depicted, Figs. S4A and D are the SEM and TEM images of CNTs; Figs. S4B and E are the SEM and TEM images of PDA-CNTs, respectively. Compared with CNTs, it can be clearly seen that there were spherical dopamine polymers on the CNTs, indicating the successful preparation of PDA-CNTs, which were further verified by the FTIR spectra of DA, CNTs, and PDA-CNTs in Fig. S4F. As shown, the PDA-CNTs possessed the characteristic peaks at 1200–1600 cm^{-1} for DA and hydroxyl peaks at 3500 cm^{-1} for CNTs, which further demonstrated the success preparation of the PDA-CNTs [27]. Additionally, the SEM image of agarose gel electrolyte doped with PDA-CNTs in Fig. S4C suggested the successful doping of PDA-CNTs into the agarose gel electrolyte.

As depicted in Fig. 1A, the original agarose gel electrolyte exhibited suboptimal water retention at body temperature, maintaining less than 50% of its moisture content after 10 h and dwindling to a mere 10% after 20 h, eventually leading to complete dehydration within one day. This rapid loss of hydration rendered the initial agarose gel electrolyte unsuitable for WFSDs, as it failed to maintain its functionality over an adequate period. However, the introduction of PDA-CNTs significantly enhanced the hydrophilic character of the agarose electrolyte, quintupling the water retention capacity. Subsequently, the agarose gel electrolyte doped with PDA-CNTs could preserve 51% of its water content even after 50 h at body temperature. This significant improvement ensured that the agarose gel electrolyte doped with PDA-CNTs was a viable option for prolonged use in WFSDs, offering improved durability and consistent performance.

In the compression strength analysis presented in Fig. 1B, the agarose gel electrolyte doped with PDA-CNTs demonstrated remarkable improvements in mechanical stability. The optimized hydrogel's resistance to compressive forces saw a significant increase, with the maximum load bearing capacity soaring from 1954.06 N to an impressive 5464.66 N. This substantial augmentation in compressive resilience ensures that the hydrogel electrolyte was considerably tougher and less susceptible to cracking under the strain of daily activities. This advancement rendered it a much more practical and reliable candidate for incorporation into wearable technology applications.

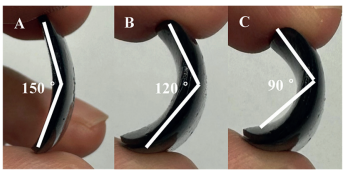

Fig. 2. Bending test of agarose gel electrolytes doped with PDA-CNTs: (A) 30°, (B) 60°, (C) 90°.

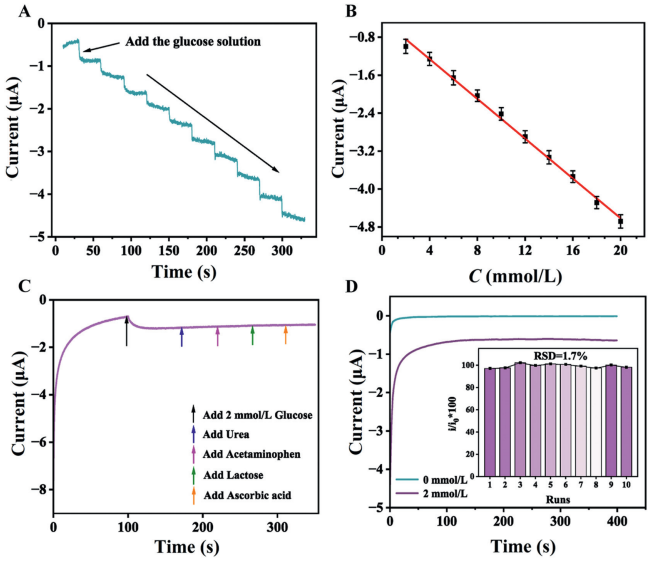

Fig. 3. (A) The *I-t* response of GOx-SPC obtained by the continuous addition of the same concentration of glucose. (B) Linear fitting of currents with glucose concentrations. (C) The interference test of GOx-SPC by the addition of 2 mmol/L glucose, 6.81 mmol/L urea, 0.5 mmol/L acetaminophen, 5.6 mmol/L lactose and 0.5 mmol/L ascorbic acid in turn. (D) The *I-t* response stability of the SPC under 0 and 2 mmol/L glucose (Inset represents the stability of the SPC obtained by I/I_0).

Fig. 1C illustrates the pressure retention of the agarose gel electrolyte doped with PDA-CNTs when subjected to a prolonged exposure at physiological temperature. Impressively, even after an extended period of 45 h, the agarose gel electrolyte doped with PDA-CNTs pressure retention stood at 95.89% relative to its original state, underscoring the gel's stability and durability under conditions mimicking human body temperature. The EIS Nyquist plots presented in Fig. 1D reveal lower impedance for the agarose gel electrolyte doped with PDA-CNTs. This observation suggested that the incorporation of CNTs increased [28] the electrical conductivity of the agarose gel electrolyte.

Furthermore, Fig. 2 shown the excellent flexibility of the agarose gel electrolyte doped with PDA-CNTs. These degrees were emblematic of the natural movements encountered in daily wear scenarios, indicating that the agarose gel electrolyte doped with PDA-CNTs did not break. The enhancement observed in the agarose gel electrolyte was attributed to the hydrophilicity of PDA-CNTs, which facilitates superior water retention within the gel [29]. Meanwhile, the abundant catechol groups on polydopamine enable hydrogen bonding and π-π interactions among them, which impart superior compressive strength to the PDA-CNT doped agarose hydrogel electrolyte [30].

Therefore, the PDA-CNTs not only enhanced the agarose gel electrolyte's electrochemical properties but also ensured mechanical strength, making it highly suitable for everyday applications in WFSDs.

As depicted in Fig. 3A, the current-time (*I-t*) responses of the GOx-SPC upon successive 30 s intervals of glucose addition were recorded. A consistent stepwise augmentation in the current sig-

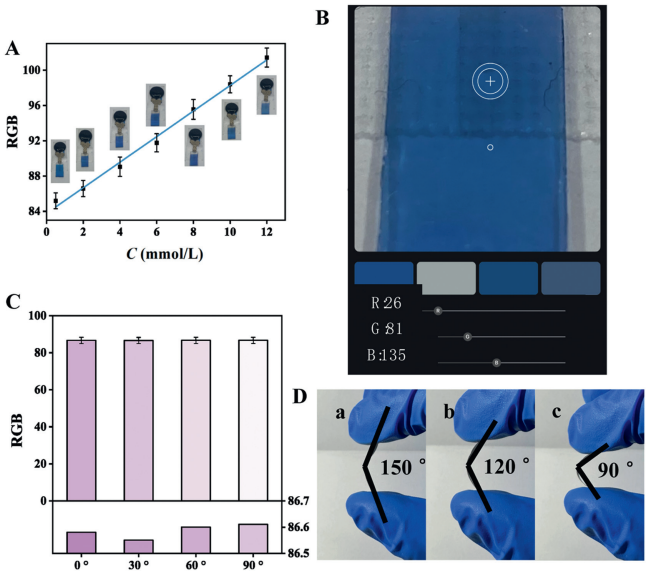

Fig. 4. (A) After adding different concentrations of glucose solution, the values of RGB were read to obtain linearity. (B) Schematic diagram of reading RGB values by selecting the color-changing area through the mobile App, and the signals stand for the values of R, G and B, respectively. (C) The bending degree test of the SPC, and its RGB was measured by bending 0°, 30°, 60° and 90°, respectively. (D) The bending degree test of the SPC at (a) 30°, (b) 60°, (c) 90°.

nal was evident with each increment of glucose. Fig. 3B presents a calibration curve illustrating the linear relationship established by the glucose concentrations and current. The derived linear calibration equation is $Y = -0.4234 - 0.2097X$ and R^2 is 0.9962. This relationship allows for precise quantification of glucose within the tested concentration range. The electrode demonstrated a robust response to varying concentrations of glucose, confirming its suitability for glucose detection applications. Fig. 3C depicts an interference study conducted with the GOx-SPC electrode. The introduction of known interferents commonly present in ISF [11], such as urea, acetaminophen, lactose, and ascorbic acid. They put into the electrolyte medium did not induce significant changed in the electrode current, underscoring the electrode's exceptional selectivity and resistance to interference.

Meanwhile, the stability of the GOx-SPC electrode was further evaluated by repeatedly measuring the current response to a 2 mmol/L glucose solution (Fig. 3D). Ten replicate measurements of the stabilized current value (I), with reference to the initial current (I_0) in the absence of glucose, were conducted. Results were expressed as the percentage of I relative to I_0, $(I/I_0) \times 100$. The RSD was calculated to be 1.7%, demonstrating the electrode's high stability. These findings indicate that the GOx-SPC electrode was a reliable sensor for glucose quantification, with potent anti-interference capabilities and stability characteristics.

Various glucose-PBS solutions (pH 7.4, 37 °C) of increasing concentrations were introduced to the GOx-SPC matrix, and the resulting colorimetric transitions were captured *via* photography (Fig. 4A). The captured images were analyzed with a smartphone application to extract RGB values, which were subsequently subjected to linear regression analysis. The linear regression equation is $Y_{RGB} = 1.450C_{Glouse} + 83.76$ ($R^2 = 0.9939$) with a linear response range of 0.5 mmol/L-12 mmol/L and a detection limit of 0.18 mmol/L (S/N = 3). The established empirical equation facilitates the translation of acquired RGB values into precise blood glucose concentrations, thereby enabling the quantification and visualization of glucose levels within biological media. Utilizing a smartphone application, a representative color block from the colorimetric transition was selected for analysis. The intensities of the red, green, and blue channels were recorded and averaged to ascertain the RGB values corresponding to the electrochromic zone, as depicted in Fig. 4B. The magnitude of the RGB values correlates positively with the degree of color change, a greater RGB value signifies a more pronounced discoloration, which, in turn, indicates an elevated glucose concentration. Employing this approach permits the quantitative assessment of glucose concentrations with visualization and accessibility.

Table 1
Comparison with standard blood glucose meters.

Sample	Blood glucose meter (mmol/L)	RGB	Calculate the corresponding value (mmol/L)	Inaccuracies (%)
1	4.2	89.69	4.087	−2.70
2	4.3	89.95	4.266	−1.00
3	4.7	90.84	4.880	3.83
4	5.2	91.45	5.300	1.92
5	5.6	91.96	5.652	0.93
6	5.8	92.17	5.800	0.00
7	6.2	92.93	6.321	1.96
8	6.8	94.00	7.058	3.79

Flexural testing was conducted on the SPC as depicted in Fig. 4C, incorporating the most prevalently utilized WFSD bending angles of 0°, 30°, 60°, and 90° [31]. The assay of RGB values reflecting glucose concentration was evaluated at a controlled level of 2 mmol/L. Statistical analysis indicated no significant deviation ($P > 0.05$) in the chromatic response of the test region post-flexure at varied angles, implying negligible effect on the determination of glucose levels. Concurrently, the adherence of the SPC to their respective substrates was meticulously assessed. In Fig. 4D, adherence evaluations of the SPC bent at angles of 30°, 60°, and 90° were performed. The results demonstrated that the SPC inks maintained robust adhesion to the PET films, with no evidence of detachment observed.

Finally, to substantiate the precision of the developed WFSD for glucose concentration monitoring, eight volunteers were recruited to ascertain their blood glucose levels 4 h postprandially, utilizing both the novel WFSD and a traditional fingertip glucometer. The RGB values procured from the WFSD were transduced into blood glucose concentration values *via* equation, and the results were juxtaposed with those obtained from the commercial glucometer (Table 1). The device was worn on the volunteers for actual sample testing and compared with the blood glucose meter respectively in Fig. S5 (Supporting information). The RGB value was recorded, and subsequently brought as in the equation to calculate exact blood glucose value. The congruence of blood glucose concentration between the sensor and the glucometer within 3.83%, thus affirming that the WFSD designed in this study met the requirements for non-invasive wearable glucose monitoring applications.

To prevent dermatological reactions during prolonged contact with the skin, the sensor's materials, including gel electrolytes, RI matching agents, and 3M medical tape were chosen for their hypoallergenic properties [32]. Fig. S6 (Supporting information) illustrated the integumentary condition post-application of the sensor for extended periods encompassing 30 min, 60 min, and 120 min. Observational assessment revealed no discernible dermal alterations, nor did the subjects report any sensations of discomfort, such as itching, attesting to the sensor's dermatological safety.

Compare with other study in Table S1 (Supporting information), the glucose in interstitial fluid was non-invasive extracted to the skin surface using reverse iontophoresis in our work, with a detection range of 0.5–12 mmol/L, which was broad, and the values can be read through color change. Moreover, the pH and temperature of our study was well with the human ISF in Fig. S7 (Supporting information). To obtain more accurate data, the most accurate data

were taken 100 s after the start of the color change and with a handheld flashlight at 2–10 cm in Fig. S8 (Supporting information).

In summary, a wearable device has been designed for detecting glucose in ISF based on a biofuel cell-driven electrochromic display. The photocurrent was generated by irradiating the photoelectric material using a handheld flashlight, and the glucose was extracted from ISF using RI. The electrochromic display changed color driven by a biofuel cell that used glucose as a biofuel and GOx as a catalyst to detect glucose. The color change of the electrochromic display can visually determine the level of blood glucose concentration and was easy to use, especially for elderly users. In addition, glucose concentration can be read by a mobile App that detect RGB values. Meanwhile, we also improved the agarose gel electrolyte by adding PDA-CNTs, which significantly improved the performance of this gel electrolyte compared with the undoped one. What is more, the prepared SPC film had excellent flexibility, which was very suitable for wearable applications. The performance of the WFSD remained unchanged under regular wearable angles. Finally, an actual sensor device sample was tested. Compared with the commercially available blood glucose meter, the blood glucose inaccuracy was within 3.83%, and it was inexpensive and did not cause symptoms such as allergy or skin damage when worn for a long period of time. Therefore, the device of this work was suitable for long-term monitoring of blood glucose levels and had good application prospects.

Ethical statement

The purpose, process, risks, and benefits of the study were explained to all individuals participating in the study, either verbally or in writing, and their informed consent was obtained. The Ethics Committee of Jiangsu University approved this study.

Declaration of competing interest

The authors declare that they have no known competing financial interests or personal relationships that could have appeared to influence the work reported in this paper.

CRediT authorship contribution statement

Kezuo Di: Writing – original draft, Visualization, Validation, Software, Project administration, Methodology, Investigation, Formal analysis, Data curation. **Jie Wei:** Writing – review & editing, Visualization, Project administration, Methodology, Investigation, Formal analysis, Conceptualization. **Lijun Ding:** Writing – review & editing, Software. **Zhiying Shao:** Writing – review & editing, Supervision, Software, Methodology, Formal analysis, Data curation, Conceptualization. **Junling Sha:** Formal analysis. **Xilong Zhou:** Software, Methodology. **Huadong Heng:** Software, Formal analysis. **Xujing Feng:** Formal analysis, Data curation. **Kun Wang:** Writing – review & editing, Supervision, Resources, Project administration, Investigation, Funding acquisition, Conceptualization.

Acknowledgments

This work was supported by the National Natural Science Foundation of China (No. 22174055), and Key R&D Program of Zhenjiang City (No. NY2022012).

Supplementary materials

Supplementary material associated with this article can be found, in the online version, at doi:10.1016/j.cclet.2024.109911.

References

[1] V. Katseli, A. Economou, C. Kokkinos, Anal. Chem. 93 (2021) 3331–3336.
[2] L. Wang, T. Xu, X. Zhang, Trac-Trend. Anal. Chem. 134 (2021) 116130.
[3] T.Q. Trung, N.E. Lee, Adv. Mater. 28 (2016) 4338–4372.
[4] Q. Lyu, S. Gong, J. Yin, J.M. Dyson, W. Cheng, Adv. Healthc. Mater. 10 (2021) 2100577.
[5] Y.C. Lin, M. Rinawati, L.Y. Chang, et al., Sens. Actuat. B: Chem. 383 (2023) 133617.
[6] Q. Yang, A. Chen, C. Li, et al., Matter 4 (2021) 3146–3160.
[7] G. Chen, Y. Li, M. Bick, J. Chen, Chem. Rev. 120 (2020) 3668–3720.
[8] X. Chen, L. Yin, J. Lv, et al., Adv. Funct. Mater. 29 (2019) 1905785.
[9] L. Zhong, L. Tang, S. Yang, et al., Anal. Chem. 94 (2022) 16738–16745.
[10] H. Wu, Y. Zhang, A.L. Kjøniksen, X. Zhou, X. Zhou, Adv. Funct. Mater. 31 (2021) 2103976.
[11] I. Jeerapan, J.R. Sempionatto, J. Wang, Adv. Funct. Mater. 30 (2020) 1906243.
[12] X. Huang, L. Zhang, Z. Zhang, et al., Biosens. Bioelectron. 124-125 (2019) 40–52.
[13] J. Wang, M. Sun, X. Pei, et al., Adv. Funct. Mater. 32 (2022) 2209697.
[14] J. Kim, I. Jeerapan, J.R. Sempionatto, et al., Acc. Chem. Res. 51 (2018) 2820–2828.
[15] X. Chen, L. Luo, Z. Zeng, et al., J. Materiom. 6 (2020) 643–650.
[16] M. Shao, X. Lv, C. Zhou, et al., Sol. Energy Mater. Sol. Cells 251 (2023) 112134.
[17] W. Wu, W.C. Poh, J. Lv, et al., Adv. Energy Mater. 13 (2023) 2204103.
[18] T.G. Yun, M. Park, D.-H. Kim, et al., ACS Nano 13 (2019) 3141–3150.
[19] H. Dai, G. Zhang, D. Rawach, et al., Energy Storage Mater. 34 (2021) 320–355.
[20] L. Lv, B. Hui, X. Zhang, Y. Zou, D. Yang, Chem. Eng. J. 452 (2023) 139443.
[21] N. Schiffmann, Y. Liang, C.E. Nemcovsky, et al., Adv. Healthc. Mater. 12 (2023) 2301053.
[22] W.T. Liu, Y.P. Cao, X.H. Zhou, D. Han, Adv. Sci. 9 (2022) 2100617.
[23] M. Friedel, I.A.P. Thompson, G. Kasting, et al., Nat. Biomed. Eng. 7 (2023) 1541–1555.
[24] L. Zheng, D. Zhu, W. Wang, et al., Sens. Actuat. B: Chem. 372 (2022) 132626.
[25] L. Lipani, B.G.R. Dupont, F. Doungmene, et al., Nat. Nanotechnol. 13 (2018) 504–511.
[26] J.R. Sempionatto, J.M. Moon, J. Wang, ACS Sens. 6 (2021) 1875–1883.
[27] Z. Sun, F.L. Guo, Y.Q. Li, et al., Compos. Part B: Eng. 236 (2022) 109848.
[28] W.T. Ding, X.Y. Jiao, Y.M. Zhao, et al., ACS Appl. Mater. Interfaces 15 (2023) 37802–37809.
[29] F. Ponzio, J. Barthès, J. Bour, et al., Chem. Mater. 28 (2016) 4697–4705.
[30] Y. Li, D. Yang, Z. Wu, et al., Nano Energy 109 (2023) 108324.
[31] P. He, J. Cao, H. Ding, et al., ACS Appl. Mater. Interface. 11 (2019) 32225–32234.
[32] M. Wang, H. Zhou, H. Du, et al., Chem. Eng. J. 446 (2022) 137163.